

Dynamical Hadron Formation in Long-Range Interacting Quantum Spin Chains


Joseph Vovrosh^{1,*}, Rick Mukherjee¹, Alvise Bastianello^{2,3} and Johannes Knolle^{1,3,4}

¹Blackett Laboratory, Imperial College London, London SW7 2AZ, United Kingdom

²Department of Physics and Institute for Advanced Study, Technical University of Munich, Garching 85748, Germany

³Munich Center for Quantum Science and Technology (MCQST), Schellingstr. 4, München D-80799, Germany

⁴Department of Physics TQM, Technical University of Munich, Garching 85748, Germany

 (Received 12 April 2022; revised 2 August 2022; accepted 15 September 2022; published 19 October 2022)

The study of confinement in quantum spin chains has seen a large surge of interest in recent years. It is not only important for understanding a range of effective one-dimensional condensed-matter realizations but it also shares some of the nonperturbative physics with quantum chromodynamics (QCD), which makes it a prime target for current quantum simulation efforts. In analogy to QCD, the confinement-induced two-particle bound states that appear in these models are dubbed mesons. Here, we study scattering events due to meson collisions in a quantum spin chain with long-range interactions such that two mesons have an extended interaction. We show how novel hadronic bound states, e.g., with four constituent particles akin to *tetraquarks*, may form dynamically in fusion events. In a natural collision their signal is weak, as elastic meson scattering dominates. However, we propose two controllable protocols that allow for a clear observation of dynamical hadron formation. We discuss how this physics can be simulated in trapped-ion or Rydberg-atom setups.

DOI: [10.1103/PRXQuantum.3.040309](https://doi.org/10.1103/PRXQuantum.3.040309)

I. INTRODUCTION

The formation of hadrons in nature has its origin in the peculiar potential energy of the constituent elementary particles, i.e., the pairwise interaction energy of quarks grows indefinitely for increasing separation. This phenomenon, called confinement, is the key feature of quantum chromodynamics (QCD) [1,2] and because of its nonperturbative nature, the QCD quantum many-body problem is one of the prime targets of recent quantum simulation efforts [3]. A time-honored way of studying interacting quantum particles takes the form of controlled scattering experiments between different types of constituents of matter, most famously at the large hadron collider [4,5].

Confinement is also important in condensed-matter physics [6–8] and can be observed, for example, in quantum spin chains [9–14], the elementary excitations of which are mesonlike bound states of domain walls. Of course, these one-dimensional (1D) models are much

simpler than the full SU(3) gauge theory of QCD but they do share some of the underlying physics. Thus, basic 1D quantum spin chains may be a first step in simulating a full treatment of the strong force. Furthermore, the simulation of quantum spin-chain models is within the capabilities of current quantum simulators, with promising first results [15–22].

Confinement has been shown to lead to exotic nonequilibrium dynamics manifest in a suppression of transport [11,23,24] and entanglement spreading [25], a long lifetime of the metastable false vacuum [26–29], and exotic prethermal phases [30–32]. Recent efforts have been made in understanding scattering events among mesons [33–35] in the short-range Ising model with both transverse and longitudinal fields. Despite the rich scattering phenomenology, this setup does not host composite excitations beyond the two-quark mesons. Therefore, the observation of deep inelastic scattering with exotic particle formation needs a richer microscopic dynamics, as can be realized, for example, by introducing heavy impurities in the short-range Ising chain [36].

In this work, we investigate another mechanism that can lead to dynamical hadron formation by addressing the transverse Ising chain with long-range interactions which, in addition to confinement [12], naturally induces interactions among mesons and hosts multimeson bound states, akin to hadrons.

*jwv18@ic.ac.uk

Published by the American Physical Society under the terms of the [Creative Commons Attribution 4.0 International](https://creativecommons.org/licenses/by/4.0/) license. Further distribution of this work must maintain attribution to the author(s) and the published article's title, journal citation, and DOI.

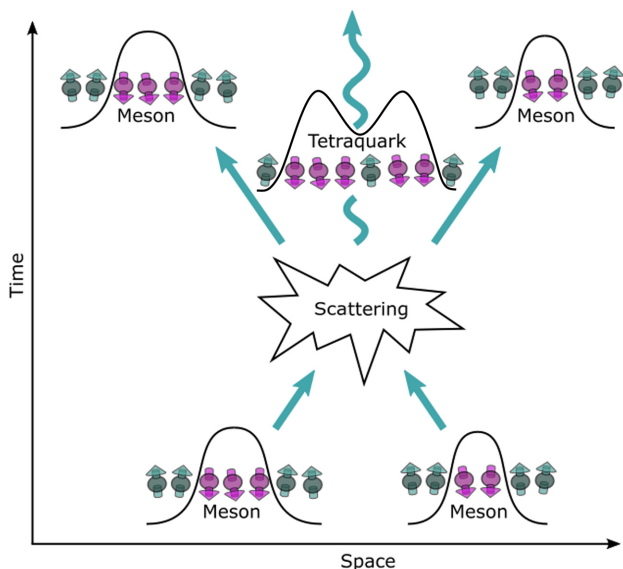


FIG. 1. A schematic of a scattering event between two wave packets of confinement-induced mesonic (two-domain-wall) states. Apart from the elastic meson reflection, the long-range interaction between the composite particles may also lead to the formation of multiparticle bound states, here in the form of a metastable four-domain-wall state akin to a tetraquark.

We show that the presence of long-range interactions between mesons can result in the formation of long-lived hadronic metastable bound states, which can form dynamically in scattering events between fundamental mesons as depicted in Fig. 1.

The resulting metastable bound states are different in nature from infinitely long-lived hadronic bound states, which cannot be excited in real-time scattering processes. Hence, natural metastable hadron formation is usually weak and the scattering events are dominated by reflection processes. To enhance the effect, we propose two different modifications of the scattering protocol. First, by an abrupt dynamical change of an external field, one can modify the kinetic energy of the mesons and induce a nontrivial overlap between the initial asymptotic states and the hadronic bound states of the postquench Hamiltonian. As a result, infinitely long-lived bound states are created and are clearly observable. Second, we consider time-independent Hamiltonians with a modified long-range spin interaction, which results in a nonmonotonic meson-meson interaction. As a result, scattering mesons can tunnel to a local minimum of the relative interaction and dynamically form a long-lived metastable bound state, which again becomes clearly observable in the collision.

Our work is structured as follows. In Sec. II, we consider the low-energy sector of the Hamiltonian by projecting on the four-domain-wall subspace. The reliability of such an approximation is related to the extremely long-lifetime of domain-wall excitations, which scales exponentially in the

weak transverse field akin to the short-range Ising chain [24]. In Sec. III, we present simulations of the real-time dynamics of a collision between two large mesons and find signatures of metastable tetraquark formation. In Sec. IV, we then show how a simple abrupt change of the kinetic energy can be utilized to allow tetraquarks to form dynamically in a more controllable setting. In Sec. V, we further show a second method of inducing fusion by performing a local alteration of the long-range interactions in the spin-chain Hamiltonian. We find that tetraquarks with a long lifetime can form dynamically without the need for a time-dependent Hamiltonian. In Sec. VI, we discuss the experimental feasibility of dynamical hadron formation in current quantum simulator platforms. In particular, we discuss initial-state preparation as well as how to implement the modified long-range spin interaction within Rydberg-atom and trapped-ion systems. Finally, we conclude with a summary and discussion.

II. HADRONS IN THE LONG-RANGE ISING MODEL

In this work, we consider the 1D Ising spin chain with long-range interactions

$$H = - \sum_{i,r} \frac{J}{r^\alpha} \sigma_i^z \sigma_{i+r}^z - h \sum_i \sigma_i^x, \quad (1)$$

where i labels lattice sites, J gives the overall energy scale (we set $J = 1$ throughout this work without loss of generality), h is the transverse-field strength, and σ_i are the Pauli matrices. The rich dynamics of the long-ranged Ising model have recently been probed in a trapped-ion quantum simulator [15], showing clear signatures of confined excitations. We are interested in the regime where the transverse field is weak: $h \ll J$. The nature of the excitation is best understood by starting with the classical model obtained for $h = 0$: here, the natural excitations are domain walls in the z magnetization and the exponent α crucially determines their interactions. In the limit of large α , the short-range Ising chain is recovered. Here, the domain walls are noninteracting objects. As α is reduced, longer-ranged domain-wall interactions are induced. In particular, two domain walls n sites apart feel an attractive potential $V(n)$ of the form [12]

$$V(n) = 4n\zeta(\alpha) - 4 \sum_{1 \leq l < n} \sum_{1 \leq r < l} \frac{1}{r^\alpha}, \quad (2)$$

where $\zeta(\alpha)$ is the Riemann zeta function. For arbitrary α , the potential $V(n)$ is a monotonically increasing function of n with a finite maximum $\lim_{n \rightarrow \infty} V(n) = V_{\max} < +\infty$ for $\alpha > 2$. In contrast, in the regime $1 < \alpha < 2$, $V(n)$ is unbounded and the energy required to pull domain walls infinitely far apart is infinite, thus showing confinement.

Finally, for $\alpha < 1$, the potential $V(n)$ diverges, signaling a transition to an infinitely long-ranged model without well-defined local excitations; therefore, we always consider the regime $\alpha > 1$. The activation of a small transverse field h has two effects: (i) the domain walls become dynamical objects and can hop along the chain, and (ii) in principle, the domain walls are no longer conserved. Nonetheless, resonances between different particle-number states are greatly suppressed for a small transverse field and can safely be neglected [24]. Thus, we can project the dynamics in subspaces with a conserved number of domain walls.

For example, in the two-domain-wall sector one can consider the basis $|j, n\rangle = |\uparrow \cdots \uparrow \downarrow_j \cdots \downarrow \uparrow_{j+n} \cdots \uparrow\rangle$. In this notation, j labels the position of the first domain wall from the left and n is the relative distance of the second domain wall with respect to the first. The projected Hamiltonian takes the form [12]

$$H = \sum_{j,n} V(n) |j, n\rangle \langle j, n| - h[|j+1, n-1\rangle + |j-1, n+1\rangle + |j, n+1\rangle + |j, n-1\rangle] \langle j, n| \quad (3)$$

and can be understood as a kinetic term for each domain wall with hopping strength h and a potential $V(n)$. As mentioned above, confinement in a strict sense requires $1 < \alpha < 2$ such that domain walls cannot be separated. Nonetheless, also for larger α , the two-kink subspace shows the presence of deep bound states and asymptotic states of freely propagating domain walls can be very high in energy and extremely difficult to excite. Therefore, as long as asymptotically propagating domain-wall states can be neglected, the dynamics of these deep two-kink bound states closely resemble those observed in the strictly confined regime and with a slight abuse of jargon, we refer to both as ‘‘mesons.’’ Due to the fact that larger values of α mitigate finite-size corrections caused by the long-range potential, we mainly focus on the regime $\alpha \sim 2.5$ but stress that similar physics appears for $1 < \alpha < 2$.

As our goal is the observation of hadronlike excitations, we need to consider interactions among mesons. We focus on the dynamics within the four-kink subspace and use a straightforward extension of the above two-domain-wall projection. We consider the basis $|j_1, n_1, j_2, n_2\rangle = |\uparrow \cdots \uparrow \downarrow_{j_1} \cdots \downarrow \uparrow_{j_1+n_1} \cdots \uparrow \downarrow_{j_2} \cdots \downarrow \uparrow_{j_2+n_2} \cdots \uparrow\rangle$, in which the projected Hamiltonian takes the shorthand form

$$H = \sum_{j_1, n_1, j_2, n_2} V(n_1) |j_1, n_1, j_2, n_2\rangle \langle j_1, n_1, j_2, n_2| + V(n_2) |j_1, n_1, j_2, n_2\rangle \langle j_1, n_1, j_2, n_2| + I(j_1, n_1, j_2, n_2) |j_1, n_1, j_2, n_2\rangle \langle j_1, n_1, j_2, n_2| - h[\text{hopping terms}]. \quad (4)$$

Here, I can be seen as the meson interaction such that [28]

$$I(j_1, n_1, j_2, n_2) = -4 \sum_{j_1 < r \leq j_1 + n_1} \sum_{j_2 < s \leq j_2 + n_2} \frac{1}{(s-r)^\alpha} \quad (5)$$

and ‘‘hopping terms’’ refers to those of the form $|j_1 \pm 1, n_1 \mp 1, j_2, n_2\rangle \langle j_1, n_1, j_2, n_2|$ or equivalently for the second meson. Note that the form of the interaction, I , depends on the choice of boundary conditions. Here, we consider open boundaries. Given two mesons of fixed widths, this effective interaction term scales as $d^{-\alpha}$ at large separation, in which $d = (j_2 - j_1 - n_1)$. Thus, similar to domain walls that are spatially distant from each other, individual mesons that are far apart from each other interact only weakly.

In Fig. 2, we show some of the lower energy levels of the four-domain-wall subspace. We clearly see large energy gaps in correspondence with internal quantum numbers, labeling the energy levels of the two-kink mesons. Additional structure is then provided by bound states of fundamental mesons and asymptotic scattering states (see the inset). In the case of deep bound states where the binding energy is much larger than the transverse field h , the two-kink mesonic wave function is very peaked on integer values of the relative distance; hence the meson has an

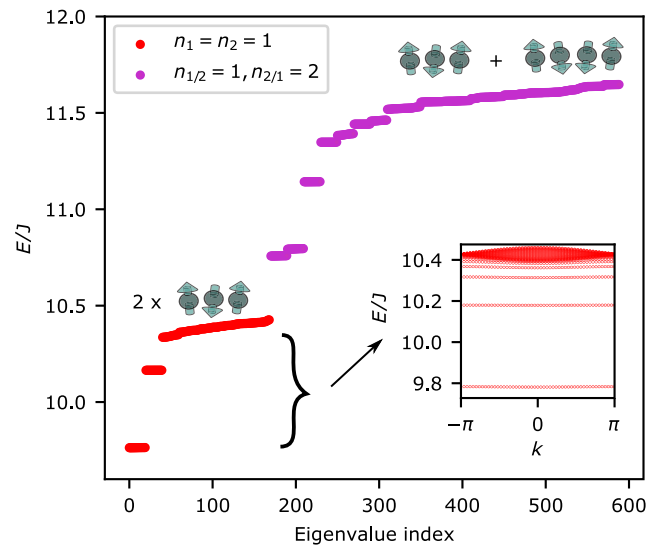


FIG. 2. The low-energy states of the four-domain-wall subspace are shown for $L = 20$, $\alpha = 2.6$, and $h = 0.1$. The energies strongly depend on the average size of the constituent mesons, resulting in large gaps between levels of different meson sizes. A schematic of the local spin configurations within each subspace is depicted above the corresponding energy level. Importantly, due to the long-range interaction, the energy within each subspace also depends on the distance between the two mesons, i.e., the closer the mesons are together, the lower is their energy. The inset shows the energies of the 1-meson subspace as a function of the momentum. The lowest energy levels in this subspace are bound states of multiple-constituent domain walls.

approximately fixed length, which is in one-to-one correspondence with the internal energy levels. In this regime, we can pictorially use the size of the meson as a good quantum number. Nonetheless, this correspondence is blurred, as bound states become shallower and domain walls can oscillate with the internal dynamics.

Before turning to real-time numerical simulations of scattering events, it is useful to comment further on the meson-meson bound-state structure, i.e., our sketch of hadrons. As shown in Fig. 2, energy levels corresponding to hadrons are clearly visible in the spectrum; their number and the gap with respect to the asymptotic scattering states depends on the “size” (i.e., the energy) of the binding mesons. These bound states are clearly orthogonal to asymptotic scattering states; hence scattering events cannot couple to them. If we wish to observe dynamical hadron formation, we should aim for metastable states arising from asymptotic scattering states the wave function of which is large when mesons are close, which means that they are qualitatively close to true bound states. Heuristically, these states are most likely to be present where the spectrum shows a smooth transition between bound states and scattering states, i.e., when the energy gap between the two is small. As it is clear from Fig. 2, this is the case for large mesons. This picture is also suggested by semiclassical arguments, since for large mesons the relative position of the kinks can oscillate. Therefore, part of the scattering energy of the two incoming mesons can be converted to internal energy of the mesons upon scattering and a bound state may form. This is not possible for tightly bound mesons, where the relative position of the kinks cannot be changed. These considerations motivate

the use of large mesons in the following natural scattering protocol.

III. INELASTIC COLLISIONS OF LARGE MESONS

We now consider the Hamiltonian projected in the four-kink subspace and numerically explore scattering events between mesons. As initial states, we choose Gaussian meson wave packets with a well-defined momentum. Furthermore, we fix the average length of each meson to cover a few lattice sites, approximately 4–10. Details on the wave-packet wave function are relegated to the Supplemental Material [37]. Simulations in the four-kink subspace are challenging for large system sizes. Therefore, we take advantage of global momentum conservation and focus on the sector with zero total momentum. Using translational invariance, we measure the kink coordinates with respect to the leftmost domain wall, which can reduce the Hilbert space dimension by a factor of L , allowing us to access much larger systems.

In the zero-momentum sector, we can then label the Hilbert space by only three variables, $|n_1, j_2, n_2\rangle$, as the first kink can be pinned to $j_1 = 0$. As a consequence of this convention, in our real-time simulation, the leftmost meson will appear stationary.

In Fig. 3(a), we show a collision event between a left meson of initial width $n_1 = 10$ and a right meson with initial width $n_2 = 4$. We employ the observable $P_K(i) = |\langle \psi | (1 - \sigma_i^z \sigma_{i+1}^z) | \psi \rangle|^2$, which can be seen as the probability that a domain wall is located at site i .

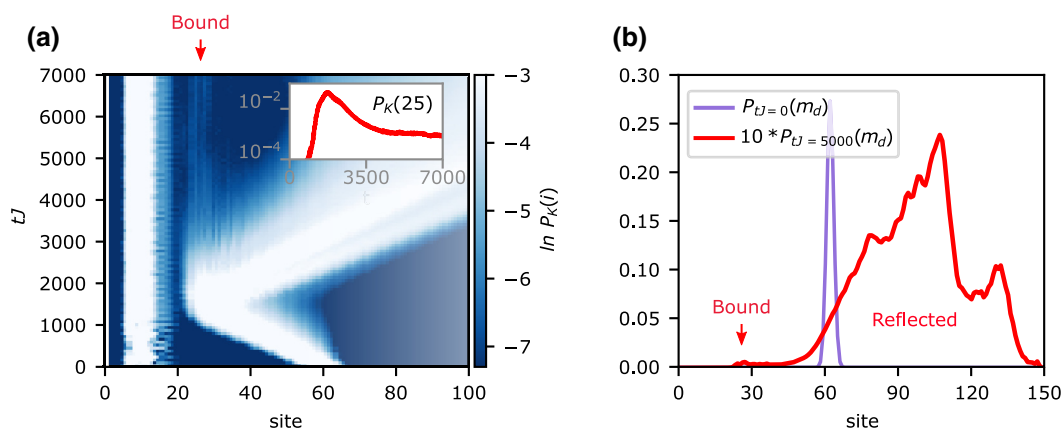


FIG. 3. The dynamical formation of a tetraquark through an inelastic collision of large mesons. Here, the Hamiltonian parameters are $L = 150$, $\alpha = 2.6$, and $h = 0.1$. The full details of the initial wave packet can be found in the Supplemental Material [37]. (a) The collision between a mobile meson initialized with a width of four sites and a stationary meson with an initial width of ten sites. Although the vast majority of the incoming wave packet is reflected, there is a subtle excitation of a tetraquark that can be seen as the faint vertical lines at approximately site 25. Furthermore, an inset plots the cross section of the time dynamics at site 25, showing the long lifetime of the tetraquark formed. Note that we choose to plot sites up to 100, as this contains the relevant information for our discussion. (b) The probability distribution of $m_d = j_2 + n_2$ at times $tJ = 0$, the initial wave packet, and $tJ = 5000$, after the collision event. After the collision, we clearly see that the majority of the wave packet is reflected; however, there is a subtle peak at approximately site 25 that corresponds to a bound tetraquark state.

In Fig. 3, we observe that scattering is dominated by elastic reflection events. However, by plotting the logarithm of the data, we are able to highlight subtle details, e.g., a small portion of the wave packet, approximately 10^{-3} , remains close to the stationary meson for a long time after the collision, which can be seen as a vertical line of intensity at approximately site 25 in Fig. 3(a). Next, we study a basic measure of the “distance” between the two mesons, $m_d = j_2 + n_2 - j_1$. In Fig. 3(b), we plot the probability distribution of m_d before ($tJ = 0$) and after the collision ($tJ = 5000$). After the collision, the distribution has two components. First, the overwhelming probability accounts for reflection events seen as the large hump for sites > 40 . However, there is a second small peak around approximately site 25, which is a signature of our sought-after metastable tetraquark state.

For all parameter and initial-state choices we explored, the signatures of dynamical tetraquark formation are weak and elastic scattering dominates. Therefore, in the following, we propose two simple extensions of the natural meson-scattering protocol that allow for an unambiguous observation of dynamical tetraquark formation.

IV. ABRUPT CHANGE IN THE TRANSVERSE FIELD

In the previous section, we only observe weak signals of a dynamically formed tetraquark state. However, true bound states are clearly present in the spectrum but, as we have already mentioned, these are orthogonal to the scattering states of our wave packet. In the following, we explore the possibility of artificially inducing nontrivial overlaps between these two classes of states through dynamical changes in the Hamiltonian. As the most basic example, we consider abrupt changes in the transverse field h at the time of collision, t^* . We note that the very nature of the hadrons obtained in this way is very different from the previously considered metastable states, because now true bound states are excited with an infinitely long lifetime. Another advantage is that within this scenario, we do not necessarily need to target large mesons, which are challenging for experiments. Therefore, we focus on small mesons, the energy levels of which are approximately in one-to-one correspondence with their length. Hence, we refer to a meson of length n as a n -meson.

In the following, we focus on the simplest case of 1-mesons. However, as one could argue that these are just simple magnons, we confirm similar physics for nontrivial 2-mesons in the Supplemental Material [37].

For a state consisting of two 1-mesons, a single spin flip naturally leaves the 1-meson subspace. Thus, in order to get an intuitive feeling about the dynamics within a restricted 1-meson Hamiltonian, we must consider higher-order processes. The derivation can be obtained through

perturbation theory, as detailed in the Supplemental Material [37]. The 1-meson subspace has the simplified basis $|j_1, j_2\rangle = |\uparrow \cdots \uparrow \downarrow_{j_1} \uparrow \cdots \uparrow \downarrow_{j_2} \uparrow \cdots \uparrow\rangle$ and the Hamiltonian is

$$H = \sum_{j_1, j_2} h_{j_2-j_1} [|j_1, j_2 + 1\rangle \langle j_1, j_2| + |j_1 - 1, j_2\rangle \langle j_1, j_2| + h.c.] + \left(U_{j_2-j_1} - \frac{4}{n^\alpha} \right) |j_1, j_2\rangle \langle j_1, j_2|. \quad (6)$$

We obtain two contributions from second-order perturbation theory: an inhomogeneous hopping term, $h_{j_2-j_1}$, and an additional effective interaction, $U_{j_2-j_1}$. We can take advantage of translational invariance and focus on the sector with global momentum k , where we define the relative distance $j = j_2 - j_1$ and the momentum-dependent Hamiltonian H_k acting on the states $|k, j\rangle$ is given by

$$H = \sum_{k, j} 2h_j \cos \frac{k}{2} [|k, j + 1\rangle \langle k, j| + h.c.] + \left(U_j - \frac{4}{j^\alpha} \right) |k, j\rangle \langle k, j|, \quad (7)$$

which we can use to calculate the energies as a function of the momentum. We note that the energies of the low-energy 1-meson sector are in very good quantitative agreement with those of the full four-domain-wall subspace as well as full exact diagonalization (ED) (see the Supplemental Material [37]).

In the inset of Fig. 2, we show the spectrum of this 1-meson subspace. One can clearly see that the lowest energy levels are discrete with large gaps between them, which correspond to bound states of two mesons that reside only a few sites away from each other; i.e., they describe tetraquarks. In addition, there is a continuum of levels at a higher energy of far-apart mesons that interact only weakly; i.e., they are free to propagate.

We implement the proposed protocol in Fig. 4. We initialize the 1-meson Gaussian wave packets with well-defined momentum and suddenly reduce the transverse field at a time t^* when the scattering takes place (dotted horizontal line in the figure). The main part of the signal indeed remains trapped in a bound state at the center of the chain, thus realizing the desired dynamical hadron-forming event.

In Fig. 5, we show the dispersion relations of the pre- and postquench Hamiltonians as a function of the total momentum k . Bound states appear as well-separated bands below a high-energy continuum of asymptotic states. Note that the bound states for $h = 0.1$ have an almost flat dispersion and hence very small velocities, which explains the trapped stationary signal observed in Fig. 4. Albeit

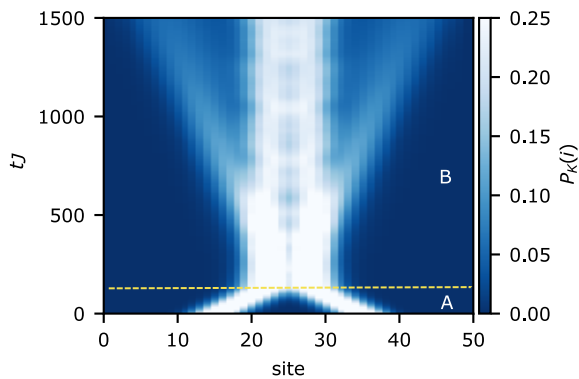


FIG. 4. The dynamical formation of a tetraquark with an abrupt change of the transverse field (calculated in the full four-domain-wall subspace). Here, the Hamiltonian parameters are $L = 50$ and for $\alpha = 2.6$. The full details of the initial wave packet can be found in the Supplemental Material [37]. In section A (up to the yellow dashed line), two 1-meson wave packets move toward each other with a large kinetic energy (transverse field $h = 0.2$). Then, at the point of meson collision ($tJ = 125$), an abrupt change to a smaller transverse field ($h = 0.1$) is performed, reducing the kinetic energy in section B. This reduction of kinetic energy can be seen by comparing the high velocity of the meson wave packets in section A to the low velocity in section B. We see that this process induces the formation of a tetraquark with exotic internal dynamics.

hardly moving, the trapped bound state is oscillating in time. In Fig. 5(b), we show that the oscillating frequencies are indeed compatible with the energy gaps between the bound-state energies of the postquench Hamiltonian.

V. MODIFIED LONG-RANGE INTERACTIONS

While the abrupt change of the transverse-field protocol is very efficient in exciting bound states, it can arguably be regarded as an artificial shortcut to our goal of observing multimeson binding in scattering events. Therefore, we now consider possible modifications of the interactions that can enhance the phenomenon without time-dependent changes.

It is again useful to focus on the 1-meson subspace and consider the relative interaction between two mesons shown in Fig. 6(a), which is a monotonically decreasing function of the relative distance (dashed line). An enhancement of bound-state trapping can then be achieved by modifying the spin interactions to form a potential well. For example, this can be achieved with the minor modification of the Hamiltonian,

$$H = - \sum_{i,r} \frac{J}{r^\alpha} \sigma_i^z \sigma_{i+r}^z - h \sum_i \sigma_j^x + \frac{J}{d^\alpha} \sum_i \sigma_i^z \sigma_{i+d}^z, \quad (8)$$

inducing a potential well in the relative potential at separation d [see the solid curve in Fig. 6(a)]. Two colliding mesons will now see a potential barrier of finite width and a

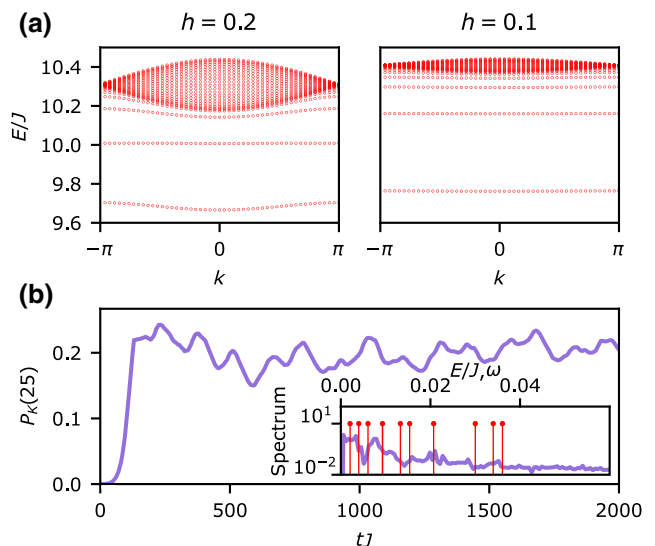


FIG. 5. An analysis of the oscillations in the fusion event shown in Fig. 4. (a) The energies of the 1-meson subspace before (left) and after (right) the change in the transverse field at the time of collision. The larger transverse field broadens the continuum of free-meson states, which corresponds to increasing their kinetic energy. (b) The time dependence of the central site 25 from Fig. 4, showing the internal dynamics of the dynamically formed tetraquark. The inset shows the spectrum of the oscillation frequencies observed. Clear agreement is seen between the dominant frequencies observed and differences in the energy levels E_i of the 1-meson subspace after the change of field to $h = 0.1$; these are shown by the vertical red lines.

quantum tunneling event may occur in the collision. In the following, we again focus on 1-mesons for simplicity but similar bound-state formation can be observed for scattering of larger mesons (see the Supplemental Material [37]). Physically, this can be understood as increasing the energy of states that have up spins d sites away from each other. In terms of the 1-meson Hamiltonian, this is equivalent to removing the interaction between mesons that are d sites away from each other.

Figure 6(b) shows the effect of the modified interaction for allowing a long-lived tetraquark to form dynamically. Here, we initialize two meson wave packets with opposite momentum. We observe, as expected, that in the presence of the effective potential well, there is a small probability that the mesons tunnel through the potential barrier, forming a metastable tetraquark decaying with a lifetime τ . We also show the results of measuring $P_{\text{TQ}}(i) = \sum_{\mathcal{C}} |\psi(j_1, n_1, j_2, n_2)|^2$, where \mathcal{C} is the set of basis states such that there is a domain wall at the i th site and $j_2 - (j_1 + n_1) \leq d$. This observable can be seen as the probability that a tetraquark is located around site i . From this we indeed see that, at the point of collision, a tetraquark forms and has a long lifetime (right panel).

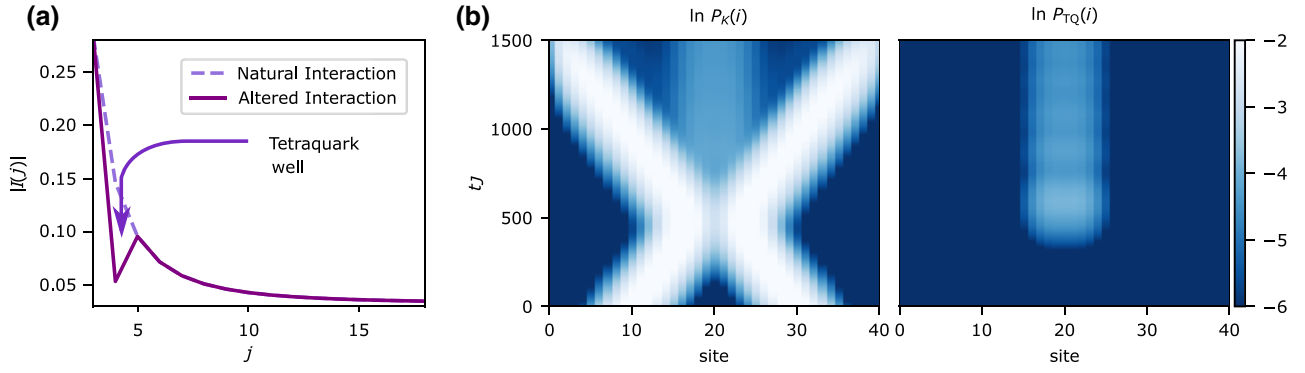


FIG. 6. The dynamical formation of a tetraquark from a collision of 1-mesons using a modified long-range interaction with an additional potential well in the form of Eq. (8), with $d = 4$. Here, the Hamiltonian parameters are $\alpha = 2.6$ and $h = 0.1$. The full details of the initial wave packet can be found in the Supplemental Material [37]. (a) The resulting meson-meson interaction is displayed as a function of the separation, which shows the formation of a tetraquark well. Note that here, $I(j) = U_j - 4/j^\alpha$. (b) In addition to the main elastic scattering channel, a small portion of the wave packet quantum tunnels into the tetraquark well, forming a long-lived tetraquark state. In the left-hand plot, we present the real-time results for $P_K(i)$ of a meson collision. Here, we see that while the majority of the incoming meson wave packets are reflected, some tunnel into the tetraquark well and persist for long times. In the right-hand plot, we explicitly show the probability of a tetraquark forming by presenting $P_{TQ}(i)$ for the same collision event.

The decay of a metastable bound state via quantum tunnelling is reminiscent of one of the first paradigms of quantum physics— α -particle decay as observed about a century ago and explained by Gamow’s famous semiclassical theory [38]. We can go one step further with our

spin-chain analogy and compare the decay times of bound tetraquarks for varying energies, which can be achieved through varying the depth of the potential well, $J/d^\alpha \rightarrow J/d^\alpha - \epsilon$. In Fig. 7(a), we plot $\sum_i P_{TQ}(i)$ to observe the decay of states initialized as a tetraquark wave packet for varying potential well depths. We observe that tetraquarks decay exponentially in time. The lifetime is longer for tetraquarks with lower energy, which is consistent with the larger potential barrier between the bound tetraquark and free-meson states.

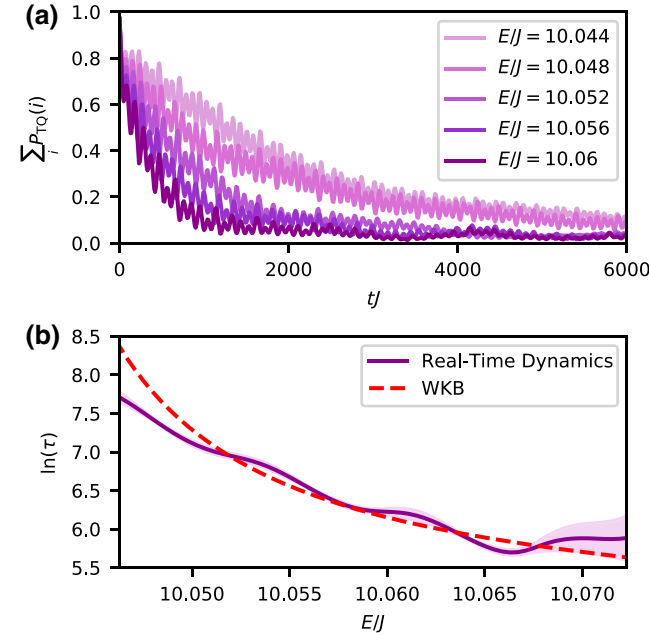


FIG. 7. The lifetime of tetraquarks varies as a function of their energy. (a) The decay of tetraquarks for various initial energies. Here, the Hamiltonian parameters are $L = 40$, $\alpha = 2.6$, and $h = 0.1$. (b) A comparison of the relationship of the natural logarithm of the lifetime, $\ln(\tau)$, of a tetraquark, calculated from the real-time simulations as well as the WKB approximation as a function of the initial energy. The WKB approximation agrees well with the lifetimes observed in the real-time dynamics.

Similar to Gamow’s theory of α -particle decay, we can utilize a WKB approximation to calculate the transmission probability of a tetraquark through the potential barrier. We note that our lattice calculation with a rapidly changing potential is beyond the strict range of applicability of any semiclassical approximation. Nonetheless, we show decent agreement with our numerical calculations, which corroborates the use of spin-chain simulators of small size for probing confinement physics.

We only summarize the results of the WKB calculation, with full details given in the Supplemental Material [37]. The transmission coefficient of a meson wave packet is

$$T(E) \propto e^{2 \int_{x_0}^{x_1} q(x) dx}, \quad (9)$$

where x_0 and x_1 are the classical turning points of the potential well and the momentum is

$$q(x) = \ln \left[\frac{-\left(U_n - \frac{4}{x^\alpha} - E\right)}{2h_{-1}} + \frac{\sqrt{\left(U_n - \frac{4}{x^\alpha} - E\right)^2 - 4h_{-1}h_{-1}}}{2h_{-1}} \right]. \quad (10)$$

One can estimate the probability of emission at any given time by $2x_1/vT$, in which v is the average velocity of the bound state. Due to the exponential nature of T , it gives the dominating contribution to the lifetime τ , which can be predicted within the WKB theory as

$$\ln(\tau) \sim C + 2 \int_{x_0}^{x_1} q(x) dx, \quad (11)$$

with a constant C [38]. In Fig. 7(b), we show that, by fitting the constant C , we see a remarkably good agreement between the WKB-theory calculations of the lifetime of tetraquarks and those extracted from the numerical simulations up to the limit of a deep tetraquark well, $E/J < 10.045$.

VI. EXPERIMENTAL FEASIBILITY

A physical realization of our meson-scattering protocols requires the implementation of the 1D transverse-field Ising model with power-law interactions as described by Eq. (1). Although there are several platforms available for the experimental realization of long-range Ising models with hundreds of spins, e.g., with polar molecules [39,40], trapped ions [41], and Rydberg atoms [42–45], they are often realized in higher-dimensional lattices. However for 1D systems, the number of spins available for quantum simulation range from 3 to 53 for ions trapped in a Paul trap [46–49] or 20–51 in the case of trapped array of Rydberg atoms in optical tweezers [50,51], thus reaching the necessary system sizes for our scattering protocols.

In these setups, the many-body state with all spins down can be naturally realized. Then, the initial-state preparation of a pair of mesons (domains) located far apart from each other can be achieved through local quenches with the help of lasers by performing flips on one or more spins at appropriate sites. The lattice spacing and the width of the laser beam determines the size of the domains, which has been demonstrated both for trapped ions [20,52,53] and Rydberg atoms [50,51,54]. For initial states to propagate along the spin chain with well-defined momentum requires controlled nearest-neighbor spin exchange. For trapped ions, spin exchange between sites is engineered using Mølmer-Sørensen type protocols [52]. Effective transitions between $|\uparrow\rangle$ and $|\downarrow\rangle$ are driven with the help of a bichromatic laser with frequencies $\omega_{\pm} = \omega_0 \pm \Delta$ that shines upon the ion array, where Δ is the detuning of the laser field from the transition frequency ω_0 of the atomic transition $|\uparrow\rangle \leftrightarrow |\downarrow\rangle$, while for Rydberg systems, the spin exchanges are achieved either by resonant dipole-dipole interaction or by off-diagonal van der Waals flip-flop interaction between Rydberg states [55]. In some cases, spin exchange can also be induced via the standard van der Waals interaction [56].

Apart from the natural scattering dynamics of the mesons, we propose two other effective routes for the

dynamical formation of tetraquarks: (i) by abruptly changing the kinetic energy as depicted in Fig. 4 and (ii) by fusion of mesons induced via a potential well as shown in Fig. 6(a). Method (i) can be implemented by abruptly changing the time-dependent transverse field. Quench dynamics of this type are commonly executed in both systems, trapped ions [15,57] as well as Rydberg atoms [58,59]. An advantage of trapped ions is that one can easily tune the strength of the long-range interactions ($1 < \alpha < 3$) in the Ising model with the help of Raman lasers, as recently demonstrated in the investigation of domain-wall dynamics [15].

However, approach (ii) requires a nontrivial modification of the spin-spin interactions to a nonmonotonic long-range form. Such exotic potentials may not be obvious for trapped ions but in the following we sketch how they can be implemented using the highly tunable effective interactions of laser-dressed Rydberg atoms [60–63]. A dressed Rydberg atom is primarily a ground-state atom that is weakly superposed with an excited state corresponding to a large principal quantum number ($n \sim 20\text{--}100$) [64]. The amount and type of the Rydberg character in the dressed superposition state is controlled using dressing lasers that eventually determine the strength and shape of the effective potential [65,66]. Recent experimental validations of Rydberg-dressed interactions include the measurement of pairwise interaction between two atoms [67] and many-body Ising interactions [68,69], as well as distance-selective interactions [70].

The key idea for our modified long-range interaction is to construct a spin-1/2 state using two long-lived states ($|g_{\pm}\rangle$) of an atom, which can either be a pair of hyperfine ground states or a ground state and a metastable state found in alkaline-earth atoms [66]. A pair of lasers (without loss of generality, left and right circularly polarized with phases set to zero) drive the atoms from $|g_{\pm}\rangle$ states to Rydberg states $|e_{\pm}\rangle$ off resonantly with detunings Δ_{\pm} and Rabi frequencies Ω_{\pm} . The full Hamiltonian in the atomic basis is $H = \sum_i (H_i^A + H_i^L) + \sum_{i<j} H_{ij}^{\text{vdW}}$, where the individual terms are the following:

$$H_i^A = -\Delta_+ |e_+\rangle_i \langle e_+| - \Delta_- |e_-\rangle_i \langle e_-|, \quad (12)$$

$$H_i^L = \frac{\Omega_+}{2} |g_-\rangle_i \langle e_+| + \frac{\Omega_-}{2} |g_+\rangle_i \langle e_-|, \quad (13)$$

$$H_{ij}^{\text{vdW}} = V(\mathbf{r}_{ij}) |e_{\alpha}\rangle_i \langle e_{\alpha}| \otimes |e_{\alpha'}\rangle_j \langle e_{\alpha'}|, \quad (14)$$

where $V(\mathbf{r}_{ij}) = C_6(\theta, \phi)/r_{ij}^6$ is the van der Waals interaction between Rydberg atoms located at sites i and j and $\alpha, \alpha' \in \{\pm\}$. The effective spin-spin interactions between two atoms can then be obtained with respect to their ground states in the weak-coupling limit $\Omega_{\pm} \ll E_{\alpha, \alpha'}$, where $E_{\alpha, \alpha'}$ are the eigenenergies of the relevant atomic systems, $H_i^A + H_i^L + H_{ij}^{\text{vdW}}$. Using perturbation theory, one derives the effective interactions between the ground states, which are

expressed in the two-atom basis as follows:

$$H_{\text{eff}} = \sum_{\substack{\alpha, \beta \\ \alpha', \beta'}} \tilde{V}_{\alpha', \beta'}^{\alpha, \beta}(\Omega_{\pm}, \Delta_{\pm}, V(\mathbf{r}_{ij})) |g_{\alpha} g_{\beta}\rangle_{ij} \langle g_{\alpha'} g_{\beta'}|. \quad (15)$$

The second-order terms in the perturbation theory correspond to light shifts that serve as longitudinal fields for the spin Hamiltonian, while the fourth-order terms provide the Ising interaction and transverse-field term. The anisotropy in the van der Waals interaction depends on the magnetic quantum numbers and the relative angles (θ, ϕ) between the atoms with respect to the laser.

Overall, our main point is that there is sufficient tunability of the spatial interaction profile in order to engineer a local minimum of the effective interaction similar to the one of Fig. 6. However, while this effective modified potential between mesons can be achieved through the van der Waals interactions, its asymptotic decay $1/r_{ij}^6$ is not enough to ensure the stability of individual meson states. In order to stabilize them, one can exploit the long-range dipole-dipole interactions that are also present. For this purpose, one then needs to consider both levels of the two-level system as Rydberg states, for which bound states have indeed been shown to exist [71]. Alternatively, switching on a weak longitudinal field would also ensure the formation of individual meson states while their mutual interaction would be governed by the longer-range potential discussed above.

A detailed quantitative modeling of experimental protocols is beyond the scope of this work; however, we provide here some estimate for coherence times. In case of Rydberg-dressed setups, the typical values of the Rabi frequencies are in the range of tens of kilohertz to a few megahertz, while the detunings are an order of magnitude larger. Rydberg states in the range of $n = 50\text{--}70$ for Rb atoms will have bare lifetimes around $80\text{--}130 \mu\text{s}$ [72]. However, as a result of the weak coupling to Rydberg states, the lifetime of the effective two-level system is extended to milliseconds [70]. For such Rydberg states, the interactions are on the order of gigahertz [72] and thus for lattice spacings of $0.5\text{--}1.5 \mu\text{m}$, one can simulate effective spin-spin interactions that are on the order of few kilohertz [68] to hundreds of kilohertz [67]. Assuming $J = 800 \text{ kHz}$ and that the time of scattering occurs at $tJ = 100$ (after optimization of the protocol dynamics), coherence times of 0.125 ms are well within the reach of many-body Rydberg-dressed state lifetimes [70]. Although the dynamical time scales shown in this theoretical work are beyond what has previously been observed in experiments, the use of quantum optimal control theory [73–75] to reduce these time scales is promising, especially with the access to a variety of control parameters such as maximizing the transverse field \hbar while maintaining the domain-wall approximation, minimizing the initial meson separation, and tuning the

initial meson size and exponent α . Indeed, achieving the dynamical time scales and coherence times needed for this work is a challenge for future experiments.

VII. CONCLUSIONS

We show that confinement-induced bound states of many elementary domain-wall excitations exist in the long-range Ising model, akin to composite hadronic particles in QCD. We study the collision of simple two-particle mesonic bound states and find signatures of the dynamical formation of metastable four-domain-wall states in analogy to tetraquarks. However, natural meson collisions are mainly elastic and the signal for natural hadron formation is weak. Therefore, we propose two alternative protocols to induce dynamical fusion events in the long-range Ising model that are much more controllable and allow for an unambiguous detection of dynamical hadron formation.

First, we show that an abrupt change in the transverse field at the time of collision results in a strong signal of tetraquark formation with interesting internal dynamics. Second, we find that a modification of the long-range interaction leads to a tetraquark potential well. Again, we obtain a clear signal of hadron formation and subsequent decay that can be understood via a semiclassical WKB approximation in analogy to the famous example of α -particle decay.

Finally, we argue that all three of these methods, while challenging, are in principle realizable with current quantum simulator setups. In particular, we sketch the experimental requirements for initial-state preparation as well as the use of laser-dressed Rydberg atoms for engineering the modified long-range interactions.

Our work motivates a number of future research questions. For example, we focus on the limit in which the elementary low-energy excitations are well approximated by domain walls. However, it is well known that for the short-range transverse-field Ising part of our Hamiltonian, domain walls continuously evolve into fermionic excitations beyond the small transverse-field regime. It would be interesting to gain insights departing from the limit of extremely weak transverse field where, most likely, sharp domain walls will be deformed similarly to what happens in the short-range Ising upon activation of a finite transverse field.

A next step toward the long-time goal of understanding fusion events in full QCD would be the quantum simulation of scattering events with dynamical hadron formation in Hamiltonians that lead to nonmesonic hadrons, such as the q -state Potts model with $q > 2$ ($q = 2$ corresponds to the Ising model) [76–79]. Furthermore, one could also consider simplified lattice-gauge theories (LGTs). For example, 1D versions of U(1) LGTs have been studied intensively in recent years, with many connections to quantum simulation architectures [19,20]. A prime candidate would

be the 1D Schwinger model, in which the confinement dynamics can be studied efficiently with time-dependent density-matrix-renormalization-group (DMRG) methods [80]. In the longer run, similar albeit richer physics is expected in higher-dimensional confining LGTs.

We hope that the emulation of particle-physics scattering experiments in toy models, the realization of which is feasible for current quantum simulators, can provide a first step toward a better understanding of the fascinating physics of large hadron collider. As quantum simulators are slowly but surely increasing in size and quality, the simulation of dynamical hadron formation in 1D and beyond would also provide a crucial benchmark toward achieving a genuine quantum advantage.

ACKNOWLEDGMENTS

We are grateful for valuable discussions with Sean Greenaway and Hongzheng Zhao. J.V. acknowledges the Samsung Advanced Institute of Technology Global Research Partnership and travel support via the Imperial—Technical University of Munich (TUM) flagship partnership. The research is part of the Munich Quantum Valley, which is supported by the Bavarian state government with funds from the Hightech Agenda Bayern Plus. A.B. acknowledges support from the Deutsche Forschungsgemeinschaft (DFG, German Research Foundation) under Germany’s Excellence Strategy—EXC–2111–390814868.

-
- [1] V. D. Barger and R. J. Phillips, *Collider Physics* (CRC Press, Boca Raton, 2018).
- [2] J. Greensite, *An Introduction to the Confinement Problem* Vol. 821 (Springer, Heidelberg, 2011).
- [3] M. C. Bañuls and K. Cichy, Review on novel methods for lattice gauge theories, *Rep. Prog. Phys.* **83**, 024401 (2020).
- [4] W. Busza, K. Rajagopal, and W. van der Schee, Heavy ion collisions: The big picture and the big questions, *Annu. Rev. Nucl. Part. Sci.* **68**, 339 (2018).
- [5] P. Campana, M. Klute, and P. Wells, Physics goals and experimental challenges of the proton-proton high-luminosity operation of the LHC, *Annu. Rev. Nucl. Part. Sci.* **66**, 273 (2016).
- [6] B. M. McCoy and T. T. Wu, Two-dimensional Ising field theory in a magnetic field: Breakup of the cut in the two-point function, *Phys. Rev. D* **18**, 1259 (1978).
- [7] G. Delfino, G. Mussardo, and P. Simonetti, Non-integrable quantum field theories as perturbations of certain integrable models, *Nucl. Phys. B* **473**, 469 (1996).
- [8] G. Delfino, P. Grinza, and G. Mussardo, Decay of particles above threshold in the Ising field theory with magnetic field, *Nucl. Phys. B* **737**, 291 (2006).
- [9] B. Lake, A. M. Tsvelik, S. Notbohm, D. Alan Tennant, T. G. Perring, M. Reehuis, C. Sekar, G. Krabbes, and B. Büchner, Confinement of fractional quantum number particles in a condensed-matter system, *Nat. Phys.* **6**, 50 (2010).
- [10] R. Coldea, D. A. Tennant, E. M. Wheeler, E. Wawrzynska, D. Prabhakaran, M. Telling, K. Habicht, P. Smeibidl, and K. Kiefer, Quantum criticality in an Ising chain: Experimental evidence for emergent E8 symmetry, *Science* **327**, 177 (2010).
- [11] M. Kormos, M. Collura, G. Takács, and P. Calabrese, Real-time confinement following a quantum quench to a non-integrable model, *Nat. Phys.* **13**, 246 (2017).
- [12] F. Liu, R. Lundgren, P. Titum, G. Pagano, J. Zhang, C. Monroe, and A. V. Gorshkov, Confined Quasiparticle Dynamics in Long-Range Interacting Quantum Spin Chains, *Phys. Rev. Lett. The APS Journals that need article titles to be title case are PRX Quantum, PRX Energy, Phys. Rev. Lett., Phys. Rev. X, and Phys. Rev. Appl.* **122**, 150601 (2019).
- [13] S. B. Rutkevich, On the weak confinement of kinks in the one-dimensional quantum ferromagnet CoNb_2O_6 , *J. Stat. Mech.: Theory Exp.* **2010**, P07015 (2010).
- [14] J. A. Kjäll, F. Pollmann, and J. E. Moore, Bound states and E8 symmetry effects in perturbed quantum Ising chains, *Phys. Rev. B* **83**, 020407 (2011).
- [15] W. L. Tan, P. Becker, F. Liu, G. Pagano, K. S. Collins, A. De, L. Feng, H. B. Kaplan, A. Kyprianidis, R. Lundgren, W. Morong, S. Whitsitt, A. V. Gorshkov, and C. Monroe, Domain-wall confinement and dynamics in a quantum simulator, *Nat. Phys.* **17**, 742 (2021).
- [16] J. Vovrosh and J. Knolle, Confinement and entanglement dynamics on a digital quantum computer, *Sci. Rep.* **11**, 11577 (2021).
- [17] J. Vovrosh, K. E. Khosla, S. Greenaway, C. Self, M. S. Kim, and J. Knolle, Simple mitigation of global depolarizing errors in quantum simulations, *Phys. Rev. E* **104**, 035309 (2021).
- [18] G. Vidal, Efficient Simulation of One-Dimensional Quantum Many-Body Systems, *Phys. Rev. Lett.* **93**, 040502 (2004).
- [19] M. C. Bañuls, R. Blatt, J. Catani, A. Celi, J. I. Cirac, M. Dalmonte, L. Fallani, K. Jansen, M. Lewenstein, S. Montangero, C. A. Muschik, B. Reznik, E. Rico, L. Tagliacozzo, K. Van Acoleyen, F. Verstraete, U.-J. Wiese, M. Wingate, J. Zakrzewski, and P. Zoller, Simulating lattice gauge theories within quantum technologies, *Eur. Phys. J. D* **74**, 165 (2020).
- [20] E. A. Martinez, C. A. Muschik, P. Schindler, D. Nigg, A. Erhard, M. Heyl, P. Hauke, M. Dalmonte, T. Monz, P. Zoller, and R. Blatt, Real-time dynamics of lattice gauge theories with a few-qubit quantum computer, *Nature* **534**, 516 (2016).
- [21] H. Bernien, S. Schwartz, A. Keesling, H. Levine, A. Omran, H. Pichler, S. Choi, A. S. Zibrov, M. Endres, M. Greiner, V. Vuletić, and M. D. Lukin, Probing many-body dynamics on a 51-atom quantum simulator, *Nature* **551**, 579 (2017).
- [22] F. M. Surace, P. P. Mazza, G. Giudici, A. Lerose, A. Gambassi, and M. Dalmonte, Lattice Gauge Theories and String Dynamics in Rydberg Atom Quantum Simulators, *Phys. Rev. X* **10**, 021041 (2020).
- [23] P. P. Mazza, G. Perfetto, A. Lerose, M. Collura, and A. Gambassi, Suppression of transport in nondisordered quantum spin chains due to confined excitations, *Phys. Rev. B* **99**, 180302 (2019).

- [24] A. Lerose, F. M. Surace, P. P. Mazza, G. Peretto, M. Collura, and A. Gambassi, Quasilocalized dynamics from confinement of quantum excitations, *Phys. Rev. B* **102**, 041118 (2020).
- [25] S. Scopa, P. Calabrese, and A. Bastianello, Entanglement dynamics in confining spin chains, *Phys. Rev. B* **105**, 125413 (2022).
- [26] R. Verdel, F. Liu, S. Whitsitt, A. V. Gorshkov, and M. Heyl, Real-time dynamics of string breaking in quantum spin chains, *Phys. Rev. B* **102**, 014308 (2020).
- [27] G. Lagnese, F. M. Surace, M. Kormos, and P. Calabrese, False vacuum decay in quantum spin chains, *Phys. Rev. B* **104**, L201106 (2021).
- [28] M. Collura, A. De Luca, D. Rossini, and A. Lerose, Discrete time-crystalline response stabilized by domain-wall confinement (2021), [ArXiv:2110.14705](https://arxiv.org/abs/2110.14705).
- [29] O. Pomponio, M. A. Werner, G. Zaránd, and G. Takacs, Bloch oscillations and the lack of the decay of the false vacuum in a one-dimensional quantum spin chain, *SciPost Phys.* **12**, 061 (2022).
- [30] S. Birnkammer, A. Bastianello, and M. Knap, Prethermalization in confined spin chains (2022), [ArXiv:2202.12908](https://arxiv.org/abs/2202.12908).
- [31] J. C. Halimeh and V. Zauner-Stauber, Dynamical phase diagram of quantum spin chains with long-range interactions, *Phys. Rev. B* **96**, 134427 (2017).
- [32] J. C. Halimeh, V. Zauner-Stauber, I. P. McCulloch, I. de Vega, U. Schollwöck, and M. Kastner, Prethermalization and persistent order in the absence of a thermal phase transition, *Phys. Rev. B* **95**, 024302 (2017).
- [33] P. I. Karpov, G. Y. Zhu, M. P. Heller, and M. Heyl, Spatiotemporal dynamics of particle collisions in quantum spin chains (2020), [ArXiv:2011.11624](https://arxiv.org/abs/2011.11624).
- [34] A. Milsted, J. Liu, J. Preskill, and G. Vidal, Collisions of false-vacuum bubble walls in a quantum spin chain (2021), [ArXiv:2012.07243](https://arxiv.org/abs/2012.07243).
- [35] F. M. Surace and A. Lerose, Scattering of mesons in quantum simulators, *New J. Phys.* **23**, 062001 (2021).
- [36] J. Vovrosh, H. Zhao, J. Knolle, and A. Bastianello, Confinement-induced impurity states in spin chains, *Phys. Rev. B* **105**, L100301 (2022).
- [37] See the Supplemental Material at <http://link.aps.org/supplemental/10.1103/PRXQuantum.3.040309> for details for the derivation of the few-meson subspaces, details on simulations, and details of the WKB approximation for tetraquark decay.
- [38] D. J. Griffiths and D. F. Schroeter, *Introduction to Quantum Mechanics* (Cambridge University Press, Cambridge, 2018).
- [39] K.-K. Ni, S. Ospelkaus, D. Wang, G. Quéméner, B. Neyenhuis, M. H. G. de Miranda, J. L. Bohn, J. Ye, and D. S. Jin, Dipolar collisions of polar molecules in the quantum regime, *Nature* **464**, 1324 (2010).
- [40] B. Yan, S. A. Moses, B. Gadway, J. P. Covey, K. R. A. Hazzard, A. M. Rey, D. S. Jin, and J. Ye, Observation of dipolar spin-exchange interactions with lattice-confined polar molecules, *Nature* **501**, 521 (2013).
- [41] J. W. Britton, B. C. Sawyer, A. C. Keith, C.-C. J. Wang, J. K. Freericks, H. Uys, M. J. Biercuk, and J. J. Bollinger, Engineered two-dimensional Ising interactions in a trapped-ion quantum simulator with hundreds of spins, *Nature* **484**, 489 (2012).
- [42] P. Schauß, M. Cheneau, M. Endres, T. Fukuhara, S. Hild, A. Omran, T. Pohl, C. Gross, S. Kuhr, and I. Bloch, Observation of spatially ordered structures in a two-dimensional Rydberg gas, *Nature* **491**, 87 (2012).
- [43] H. Labuhn, D. Barredo, S. Ravets, S. de Léséleuc, T. Macri, T. Lahaye, and A. Browaeys, Tunable two-dimensional arrays of single Rydberg atoms for realizing quantum Ising models, *Nature* **534**, 667 (2016).
- [44] S. Ebadi, T. T. Wang, H. Levine, A. Keesling, G. Semeghini, A. Omran, D. Bluvstein, R. Samajdar, H. Pichler, W. W. Ho, S. Choi, S. Sachdev, M. Greiner, V. Vuletić, and M. D. Lukin, Quantum phases of matter on a 256-atom programmable quantum simulator, *Nature* **595**, 227 (2021).
- [45] M. O. Brown, T. Thiele, C. Kiehl, T.-W. Hsu, and C. A. Regal, Gray-Molasses Optical-Tweezer Loading: Controlling Collisions for Scaling Atom-Array Assembly, *Phys. Rev. X* **9**, 011057 (2019).
- [46] E. E. Edwards, S. Korenblit, K. Kim, R. Islam, M.-S. Chang, J. K. Freericks, G.-D. Lin, L.-M. Duan, and C. Monroe, Quantum simulation and phase diagram of the transverse-field Ising model with three atomic spins, *Phys. Rev. B* **82**, 060412 (2010).
- [47] K. Kim, M.-S. Chang, R. Islam, S. Korenblit, L.-M. Duan, and C. Monroe, Entanglement and Tunable Spin-Spin Couplings between Trapped Ions Using Multiple Transverse Modes, *Phys. Rev. Lett.* **103**, 120502 (2009).
- [48] R. Islam, C. Senko, W. C. Campbell, S. Korenblit, J. Smith, A. Lee, E. E. Edwards, C.-C. J. Wang, J. K. Freericks, and C. Monroe, Emergence and frustration of magnetism with variable-range interactions in a quantum simulator, *Science* **340**, 583 (2013).
- [49] J. Zhang, G. Pagano, P. W. Hess, A. Kyprianidis, P. Becker, H. Kaplan, A. V. Gorshkov, Z.-X. Gong, and C. Monroe, Observation of a many-body dynamical phase transition with a 53-qubit quantum simulator, *Nature* **551**, 601 (2017).
- [50] A. Omran, H. Levine, A. Keesling, G. Semeghini, T. T. Wang, S. Ebadi, H. Bernien, A. S. Zibrov, H. Pichler, S. Choi, J. Cui, M. Rossignolo, P. Rembold, S. Montangero, T. Calarco, M. Endres, M. Greiner, V. Vuletić, and M. D. Lukin, Generation and manipulation of Schrödinger cat states in Rydberg atom arrays, *Science* **365**, 570 (2019).
- [51] H. Bernien, S. Schwartz, A. Keesling, H. Levine, A. Omran, H. Pichler, S. Choi, A. S. Zibrov, M. Endres, M. Greiner, V. Vuletić, and M. D. Lukin, Probing many-body dynamics on a 51-atom quantum simulator, *Nature* **551**, 579 (2017).
- [52] P. Jurcevic, B. P. Lanyon, P. Hauke, C. Hempel, P. Zoller, R. Blatt, and C. F. Roos, Quasiparticle engineering and entanglement propagation in a quantum many-body system, *Nature* **511**, 202 (2014).
- [53] N. Friis, O. Marty, C. Maier, C. Hempel, M. Holzäpfel, P. Jurcevic, M. B. Plenio, M. Huber, C. Roos, R. Blatt, and B. Lanyon, Observation of Entangled States of a Fully Controlled 20-Qubit System, *Phys. Rev. X* **8**, 021012 (2018).
- [54] H. Labuhn, S. Ravets, D. Barredo, L. Béguin, F. Nogrette, T. Lahaye, and A. Browaeys, Single-atom addressing in

- microtraps for quantum-state engineering using Rydberg atoms, *Phys. Rev. A* **90**, 023415 (2014).
- [55] H. Schempp, G. Günter, S. Wüster, M. Weidemüller, and S. Whitlock, Correlated Exciton Transport in Rydberg-Dressed-Atom Spin Chains, *Phys. Rev. Lett.* **115**, 093002 (2015).
- [56] F. Yang, S. Yang, and L. You, Quantum Transport of Rydberg Excitons with Synthetic Spin-Exchange Interactions, *Phys. Rev. Lett.* **123**, 063001 (2019).
- [57] P. Richerme, Z.-X. Gong, A. Lee, C. Senko, J. Smith, M. Foss-Feig, S. Michalakis, A. V. Gorshkov, and C. Monroe, Non-local propagation of correlations in quantum systems with long-range interactions, *Nature* **511**, 198 (2014).
- [58] P. Schauß, J. Zeiher, T. Fukuhara, S. Hild, M. Cheneau, T. Macri, T. Pohl, I. Bloch, and C. Gross, Crystallization in Ising quantum magnets, *Science* **347**, 1455 (2015).
- [59] A. Keesling, A. Omran, H. Levine, H. Bernien, H. Pichler, S. Choi, R. Samajdar, S. Schwartz, P. Silvi, S. Sachdev, P. Zoller, M. Endres, M. Greiner, V. Vuletić, and M. D. Lukin, Quantum Kibble-Zurek mechanism and critical dynamics on a programmable Rydberg simulator, *Nature* **568**, 207 (2019).
- [60] A. W. Glaetzle, M. Dalmonte, R. Nath, I. Rousochatzakis, R. Moessner, and P. Zoller, Quantum Spin-Ice and Dimer Models with Rydberg Atoms, *Phys. Rev. X* **4**, 041037 (2014).
- [61] L. I. R. Gil, R. Mukherjee, E. M. Bridge, M. P. A. Jones, and T. Pohl, Spin Squeezing in a Rydberg Lattice Clock, *Phys. Rev. Lett.* **112**, 103601 (2014).
- [62] R. M. W. van Bijnen and T. Pohl, Quantum Magnetism and Topological Ordering via Rydberg Dressing near Förster Resonances, *Phys. Rev. Lett.* **114**, 243002 (2015).
- [63] A. W. Glaetzle, M. Dalmonte, R. Nath, C. Gross, I. Bloch, and P. Zoller, Designing Frustrated Quantum Magnets with Laser-Dressed Rydberg Atoms, *Phys. Rev. Lett.* **114**, 173002 (2015).
- [64] J. E. Johnson and S. L. Rolston, Interactions between Rydberg-dressed atoms, *Phys. Rev. A* **82**, 033412 (2010).
- [65] J. B. Balewski, A. T. Krupp, A. Gaj, S. Hofferberth, R. Löw, and T. Pfau, Rydberg dressing: Understanding of collective many-body effects and implications for experiments, *New J. Phys.* **16**, 063012 (2014).
- [66] R. Mukherjee, T. C. Killian, and K. R. A. Hazzard, Accessing Rydberg-dressed interactions using many-body Ramsey dynamics, *Phys. Rev. A* **94**, 053422 (2016).
- [67] Y. Y. Jau, A. M. Hankin, T. Keating, I. H. Deutsch, and G. W. Biedermann, Entangling atomic spins with a Rydberg-dressed spin-flip blockade, *Nat. Phys.* **12**, 71 (2016).
- [68] J. Zeiher, R. van Bijnen, P. Schauß, S. Hild, J.-y. Choi, T. Pohl, I. Bloch, and C. Gross, Many-body interferometry of a Rydberg-dressed spin lattice, *Nat. Phys.* **12**, 1095 (2016).
- [69] V. Borish, O. Marković, J. A. Hines, S. V. Rajagopal, and M. Schleier-Smith, Transverse-Field Ising Dynamics in a Rydberg-Dressed Atomic Gas, *Phys. Rev. Lett.* **124**, 063601 (2020).
- [70] S. Hollerith, K. Srakaew, D. Wei, A. Rubio-Abadal, D. Adler, P. Weckesser, A. Krukenhauser, V. Walther, R. van Bijnen, J. Rui, C. Gross, I. Bloch, and J. Zeiher, Realizing Distance-Selective Interactions in a Rydberg-Dressed Atom Array, *Phys. Rev. Lett.* **128**, 113602 (2022).
- [71] F. Letscher and D. Petrosyan, Mobile bound states of Rydberg excitations in a lattice, *Phys. Rev. A* **97**, 043415 (2018).
- [72] M. Saffman, T. G. Walker, and K. Mølmer, Quantum information with Rydberg atoms, *Rev. Mod. Phys.* **82**, 2313 (2010).
- [73] H. Rabitz, R. de Vivie-Riedle, M. Motzkus, and K. Kompa, Whither the future of controlling quantum phenomena?, *Science* **288**, 824 (2000).
- [74] J. Werschnik and E. K. U. Gross, Quantum optimal control theory, *J. Phys. B: At. Mol. Opt. Phys.* **40**, R175 (2007).
- [75] R. Mukherjee, H. Xie, and F. Mintert, Bayesian Optimal Control of Greenberger-Horne-Zeilinger States in Rydberg Lattices, *Phys. Rev. Lett.* **125**, 203603 (2020).
- [76] G. Delfino and P. Grinza, Confinement in the q -state Potts field theory, *Nucl. Phys. B* **791**, 265 (2008).
- [77] L. Lepori, G. Z. Tóth, and G. Delfino, The particle spectrum of the three-state Potts field theory: A numerical study, *J. Stat. Mech.: Theory Exp.* **2009**, P11007 (2009).
- [78] S. B. Rutkevich, Baryon masses in the three-state Potts field theory in a weak magnetic field, *J. Stat. Mech.: Theory Exp.* **2015**, P01010 (2015).
- [79] F. Liu, S. Whitsitt, P. Bienias, R. Lundgren, and A. V. Gorshkov, Realizing and probing baryonic excitations in Rydberg atom arrays (2020),.
- [80] G. Magnifico, M. Dalmonte, P. Facchi, S. Pascazio, F. V. Pepe, and E. Ercolessi, Real Time Dynamics and Confinement in the Zn Schwinger-Weyl lattice model for $1 + 1$ QED, *Quantum* **4**, 281 (2020).